Virtual Surgeries of Nasal Cavities on High-Performance Computing Systems

M. Waldmann[1,2], A. Lintermann[2,3], and W. Schröder[1,2]

[1]Institute of Aerodynamics and Chair of Fluid Mechanics,
RWTH Aachen University
[2]Jülich Aachen Research Alliance, Center for Simulation and Data Science,
RWTH Aachen University & Forschungszentrum Jülich GmbH
[3]Jülich Supercomputing Centre (JSC), Institute of Advanced Simulation (IAS),
Forschungszentrum Jülich GmbH

Motivation

RHINO
Morphological and
DIAGNOST
functional precision diagnostics of the nose

Motivation

RHINO
Morphological and
DIAGNOST
functional precision diagnostics of the nose

In-vivo diagnostics

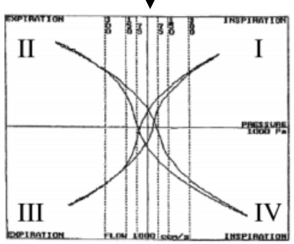

4-PR [1]

RHINO Morphological and DIAGNOST functional precision diagnostics of the nose

In-vivo diagnostics

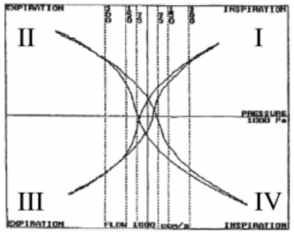

4-PR [1]

In-silico diagnostics

Geometrical Analysis

Motivation

RHINO
Morphological and
DIAGNOST
functional precision diagnostics of the nose

In-vivo diagnostics

In-silico diagnostics

Interactive Supercomputing

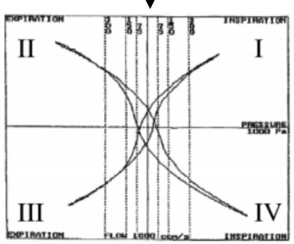

4-PR [1]

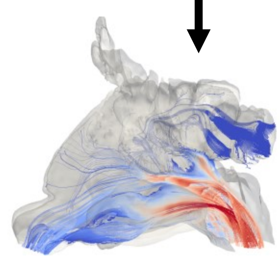

Numerical Simulation

Virtual Nose Surgery

Geometrical Analysis

$$\frac{\partial f}{\partial t} + \xi \frac{\partial f}{\partial x} + \frac{F}{m}\frac{\partial f}{\partial \xi} = \Omega_{coll}$$

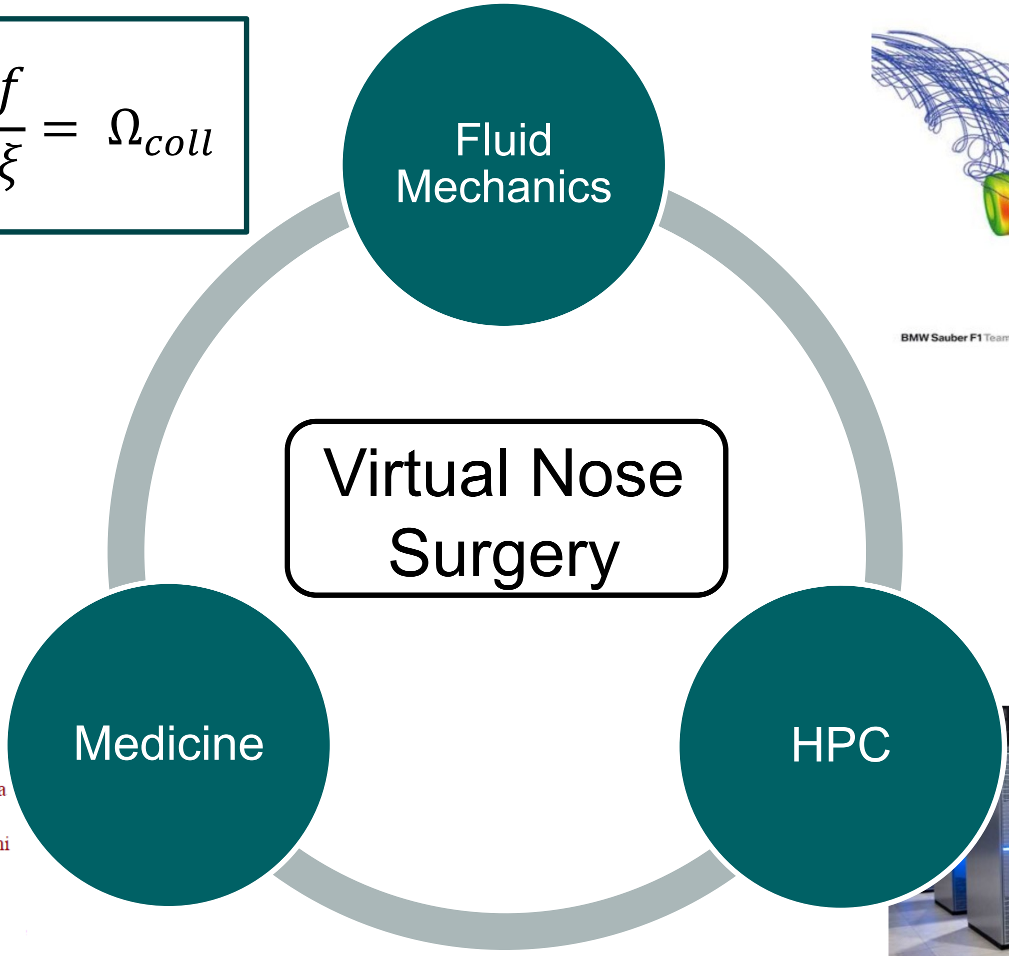

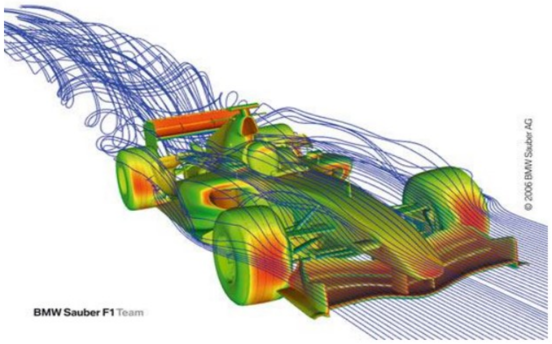

[2]

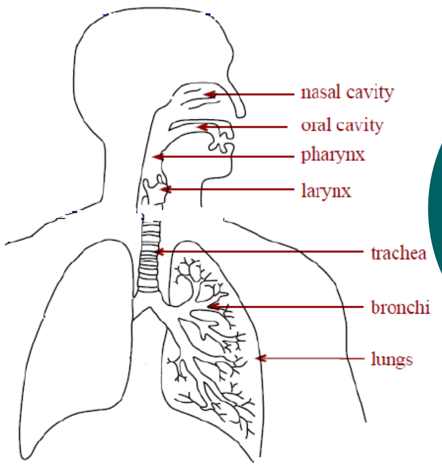

[3]

Motivation

$$\frac{\partial f}{\partial t} + \xi \frac{\partial f}{\partial x} + \frac{F}{m}\frac{\partial f}{\partial \xi} = \Omega_{coll}$$

Fluid Mechanics

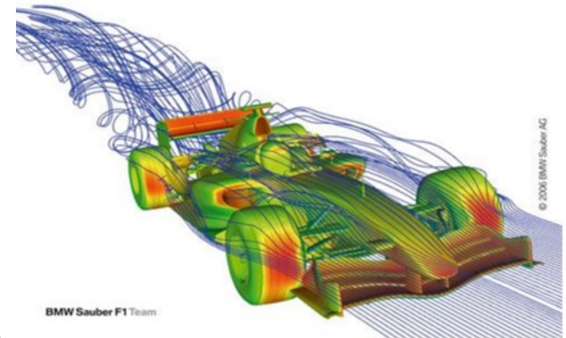

[2]

Virtual Nose Surgery

Medicine

HPC

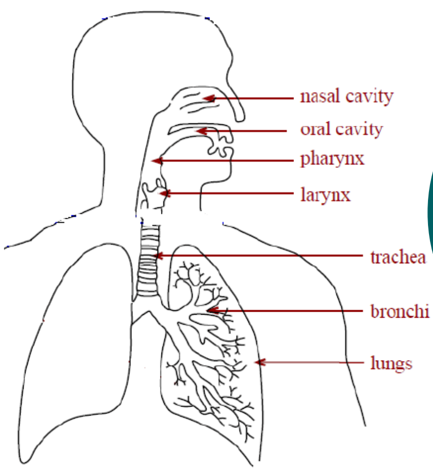

[3]

<u>Why do we need numerical methods in rhinology?</u>

Advantages of using numerical methods in rhinology:

- Three-dimensional surface geometries enable to capture the complexity of the nasal cavity
- Fluid mechanical properties determine the quality of the nasal cavity
  - The respiratory resistance is related to the total pressure loss
  - The heating capability is related to the temperature distribution

➢ **Physicians can use numerical methods to review their decision or to even find the best possible treatment**

➢ **Surgeons can conduct virtual surgery for planning and validating a surgical intervention**

Outline

- Motivation
- Numerical Methods
- Geometry Modification & Simulation Setup
- Results
- Conclusions and Outlook

Numerical Methods

Geometry acquisition:

- Realistic 3D geometries are obtained from CT-datasets in two steps [4]

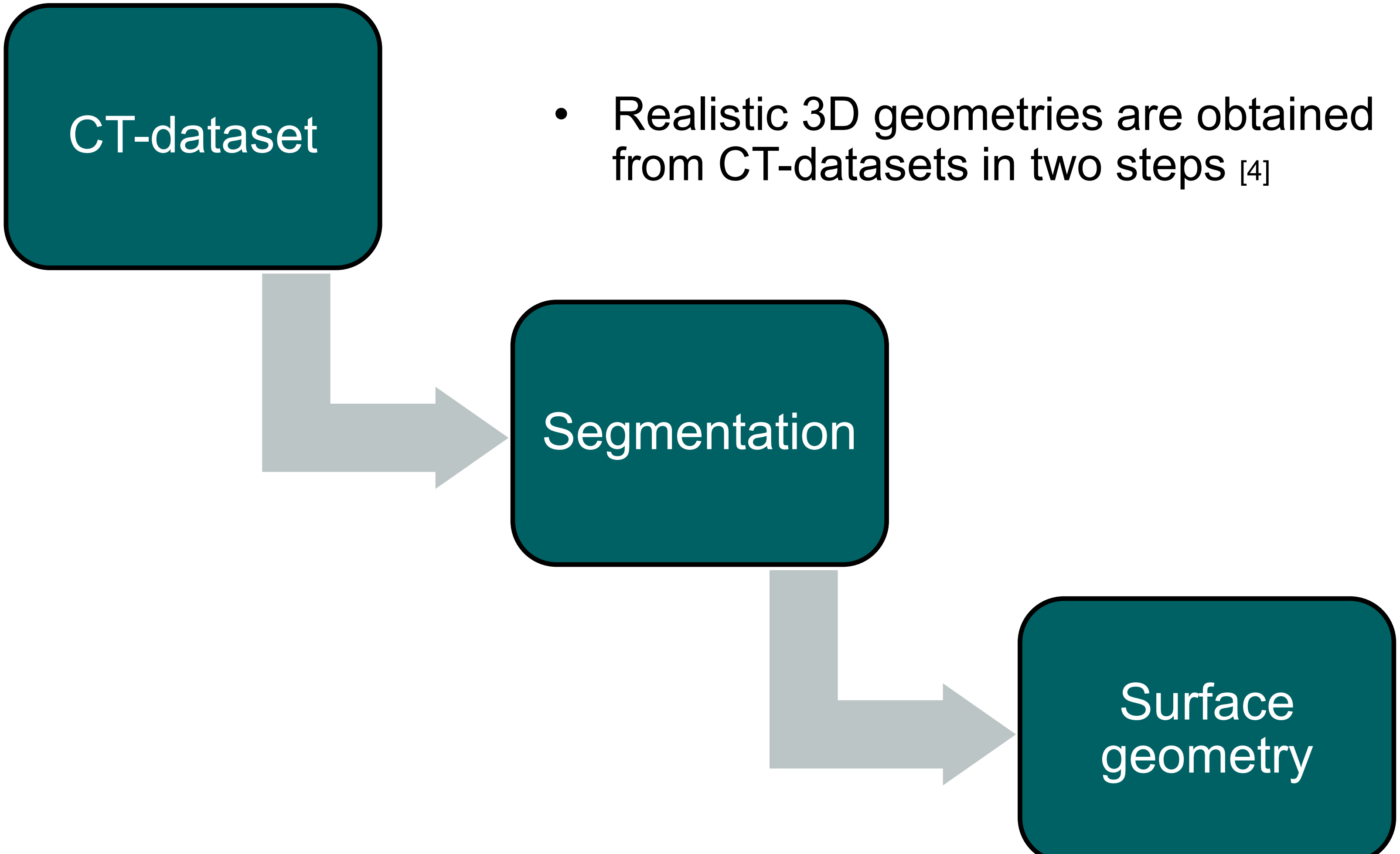

Geometry acquisition:

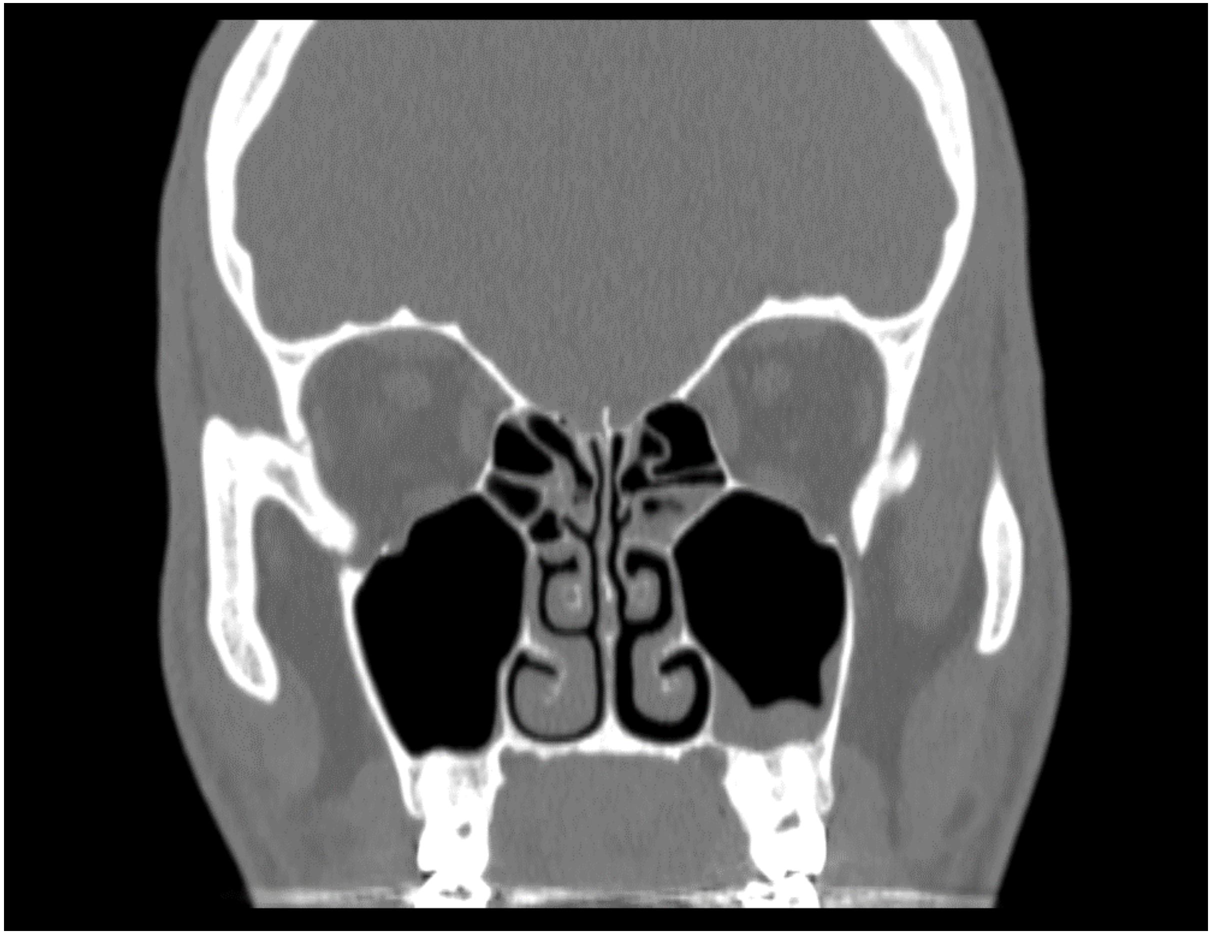

Fig 1: CT-image (coronal plane)

Geometry acquisition:

- Realistic 3D geometries are obtained from CT-datasets in two steps [4]

Segmentation

Surface geometry

Geometry acquisition:

Fig 2: Segmented data set (coronal plane)

Numerical Methods

Geometry acquisition:

- Realistic 3D geometries are obtained from CT-datasets in two steps [4]

Surface geometry

Geometry acquisition:

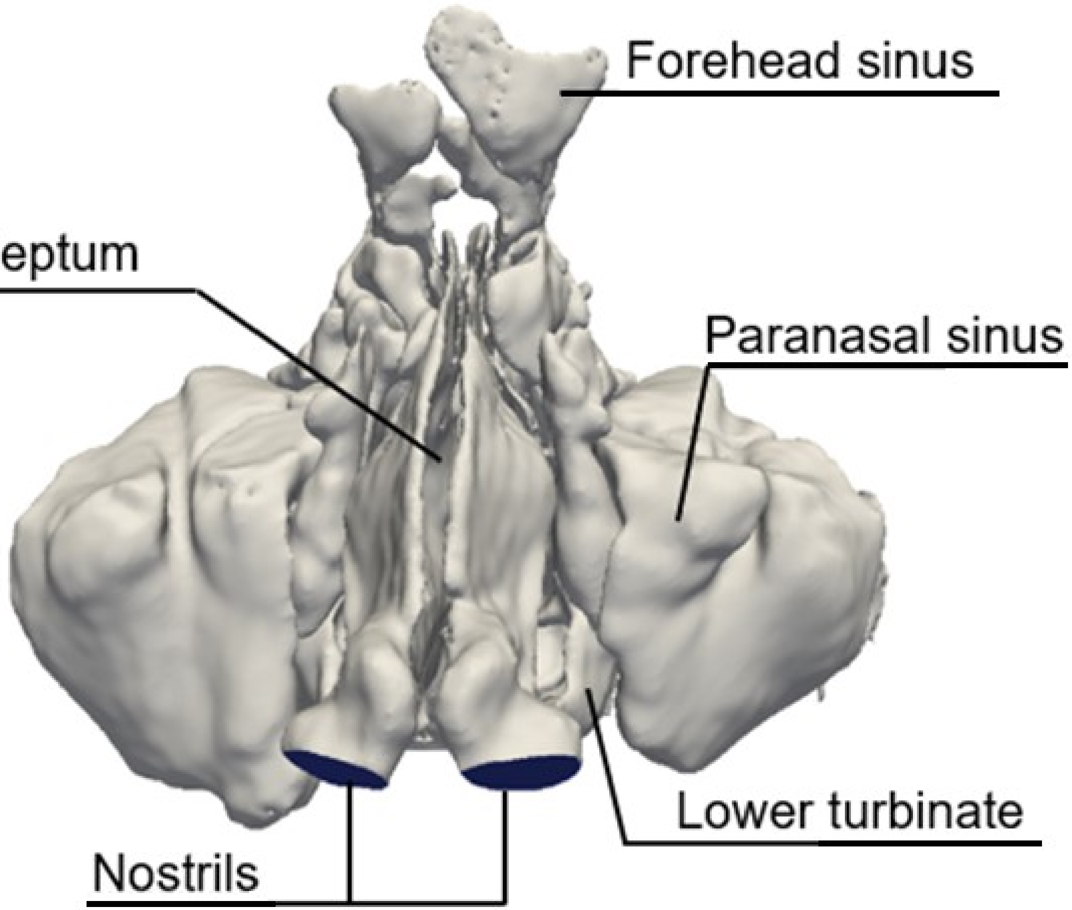

Fig 3: Water-tight 3D surface geometry

Numerical Methods

Geometry acquisition:

- Realistic 3D geometries are obtained from CT-datasets in two steps [4]

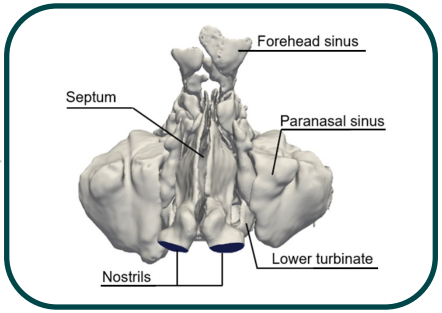

Grid generation:

- An unstructured, hierarchical Cartesian grid is generated using a massively parallel grid generator [5]

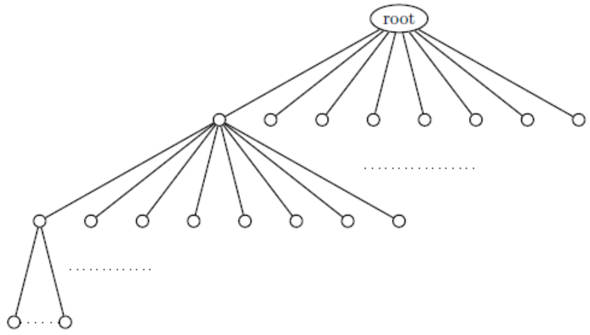

Fig 4: Octree structure [2]

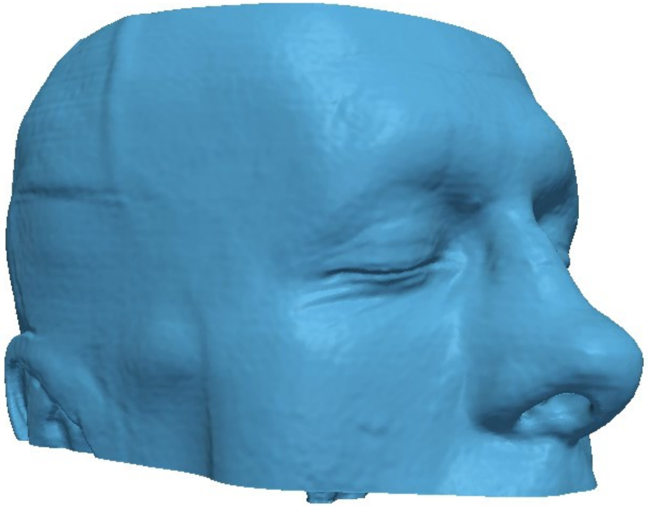

Vid 1: Massively parallel grid generator, Copyright A. Lintermann, AIA

Grid generation:

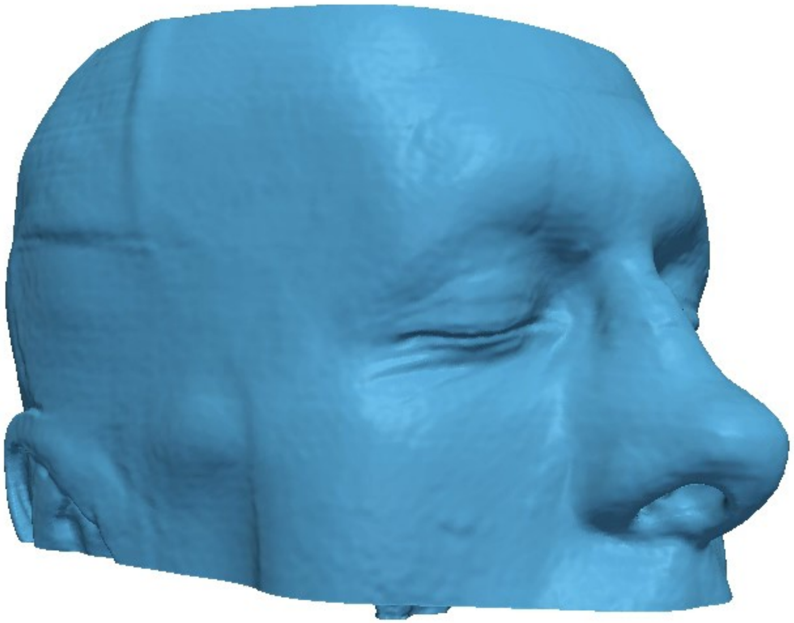

Vid 1: Massively parallel grid generator, Copyright A. Lintermann, AIA

RWTH AACHEN UNIVERSITY

Lattice-Boltzmann method:

- Solves the discrete BGK formulation of the Boltzmann equation
- $f_i\,(r,t)$ is the *Particle Probability Distribution Function* (PPDF) [6]

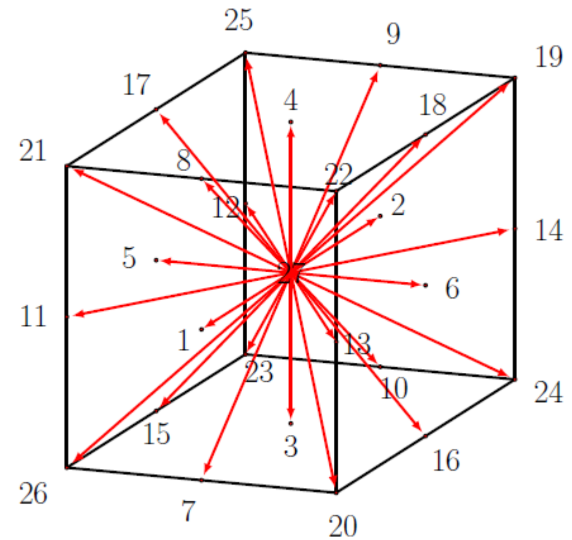

Fig 5: D3Q27 Model

$$f_i(r + \xi_i\,\delta t, t + \delta t) = f_i(r,t) - \frac{1}{\tau}\left(f_i^{eq}(r,t) - f_i(r,t)\right)$$

$$f_i^{eq} = \rho\, t_p \left(1 + \frac{v_\alpha \xi_\alpha}{c_s^2} + \frac{v_\alpha v_\beta}{c_s^2}\left(\frac{\xi_\alpha \xi_\beta}{c_s^2} - \delta_{\alpha\beta}\right)\right)$$

$$g_i(r + \xi_i\,\delta t, t + \delta t) = g_i(r,t) - \frac{1}{\tau_t}\left(g_i^{eq}(r,t) - g_i(r,t)\right)$$

$$g_i^{eq} = T\, t_p \left(1 + \frac{v_\alpha \xi_\alpha}{c_s^2} + \frac{v_\alpha v_\beta}{c_s^2}\left(\frac{\xi_\alpha \xi_\beta}{c_s^2} - \delta_{\alpha\beta}\right)\right)$$

Level-Set Method:

- The surface geometry of an arbitrary body is represented by a discrete signed *Level-Set* function
- The minimum wall distance is calculated for each cell
- Movement functions are used to simulate bodies in motion [7]
  - Translational, rotatory, and oscillating motion is possible
  - Temporal interpolation between an initial and a final *Level-Set*

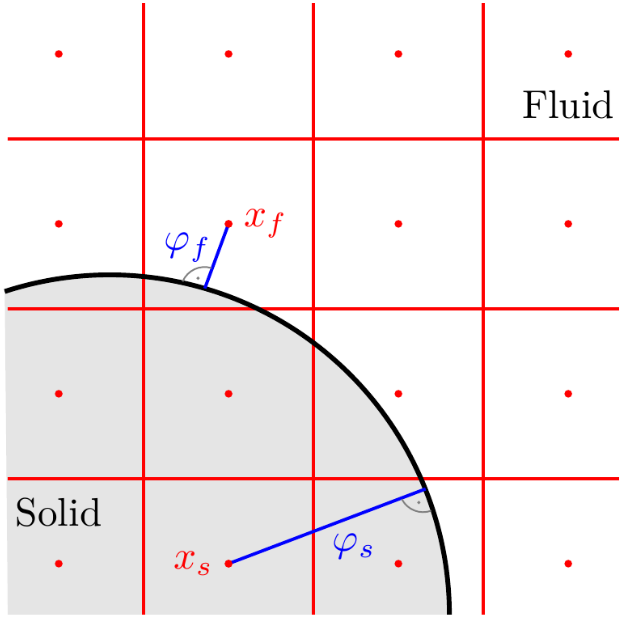

Fig 6: *Level-Set* representation of an arbitrary body

Coupled Lattice-Boltzmann-Level-Set Approach:

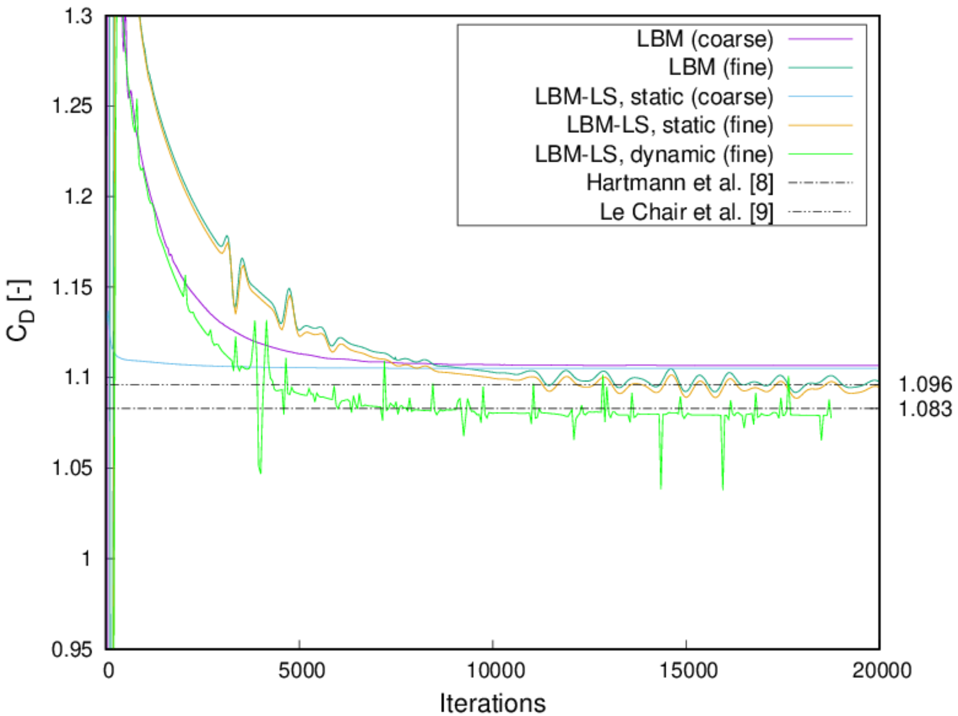

Fig 9: C_D coefficient for a sphere at Re=100

Fig 10: Static sphere at Re=100

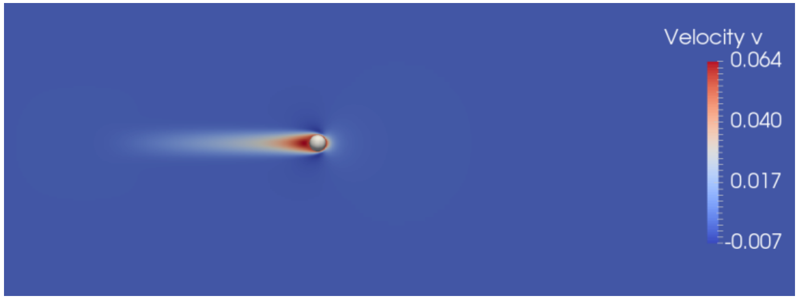

Fig 11: Moving sphere at Re=100

Coupled Lattice-Boltzmann-Level-Set Approach:

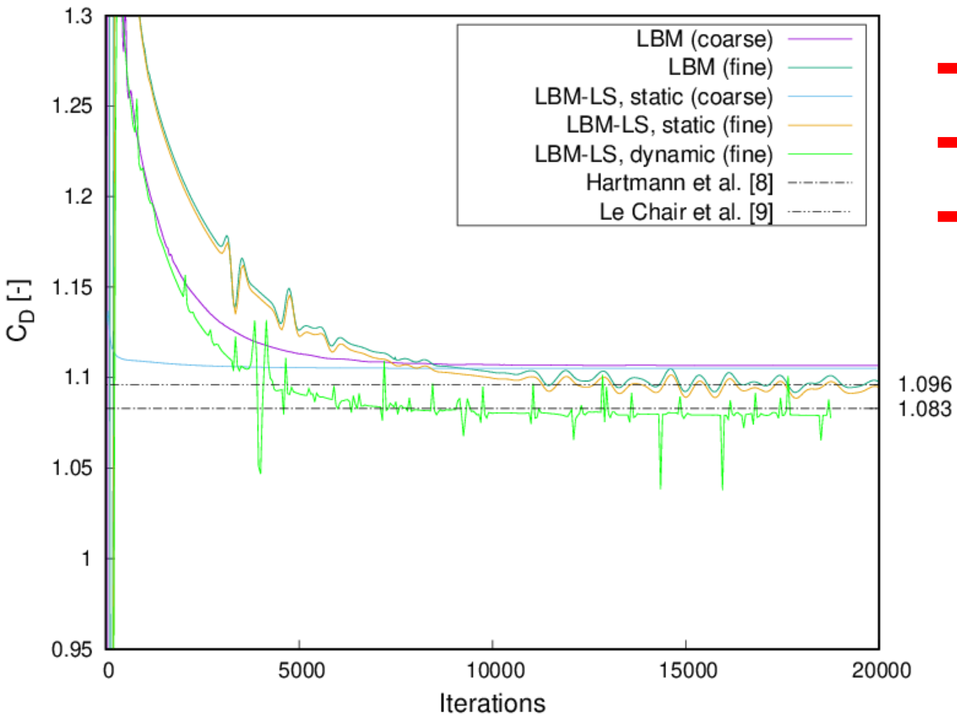

Fig 9: C_D coefficient for a sphere at Re=100

Fig 10: Static sphere at Re=100

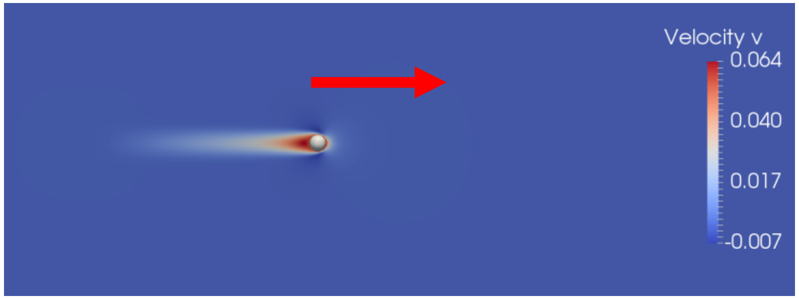

Fig 11: Moving sphere at Re=100

Outline

- Motivation
- Numerical Methods
- Geometry Modification & Simulation Setup
- Results
- Conclusions and Outlook

Geometry modification:

- The software *3D Slicer* is employed to modify the segmented data-set of a given nasal cavity
- The area between the septum and the lower turbinate was modified to demonstrate the virtual surgery
  - Simulation of a swelling
  - One of the most relevant area from a fluid mechanical point of view
  - Great impact on the respiratory resistance

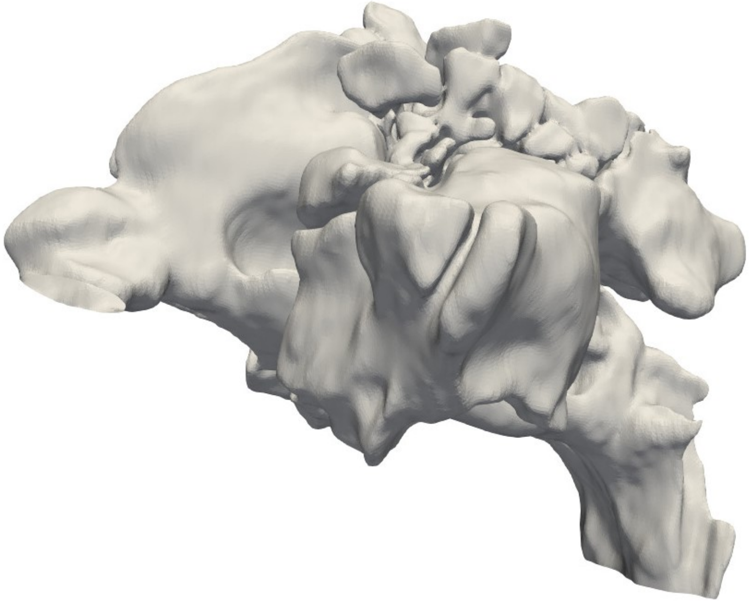

Fig 10: Nasal cavity used for virtual surgery

Geometry modification:

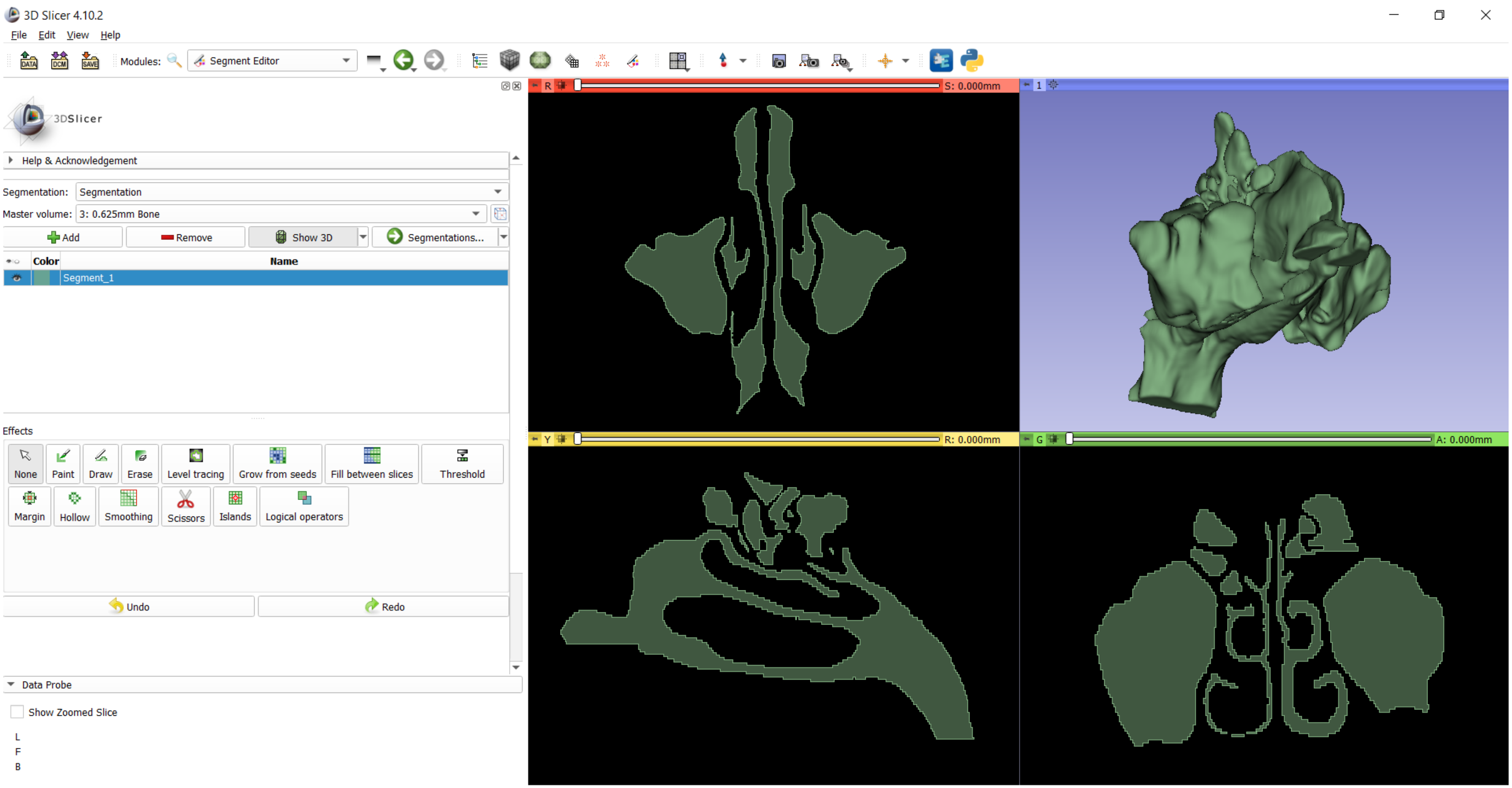

Fig 11: Screenshot of 3D Slicer

Simulation Setup

Geometry modification:

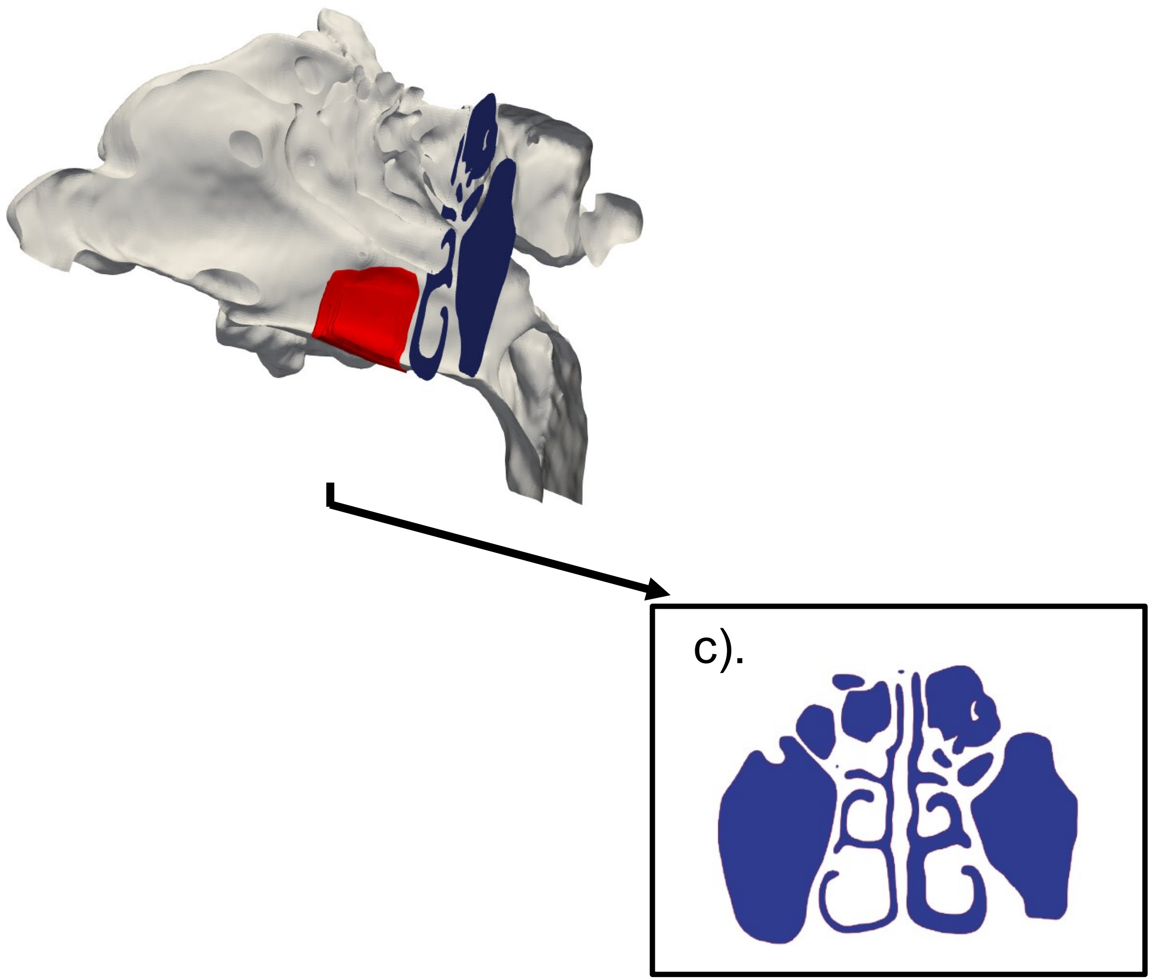

Geometry modification:

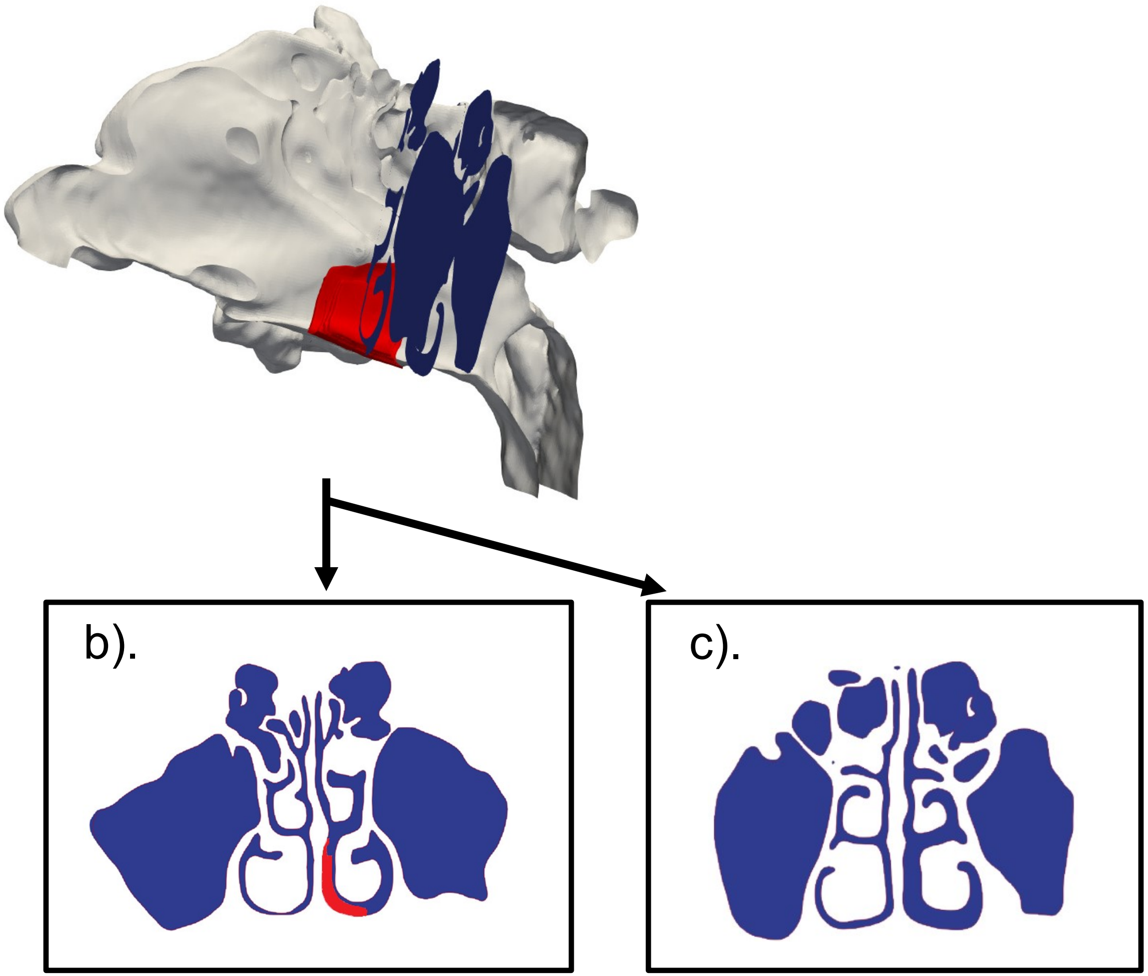

Geometry modification:

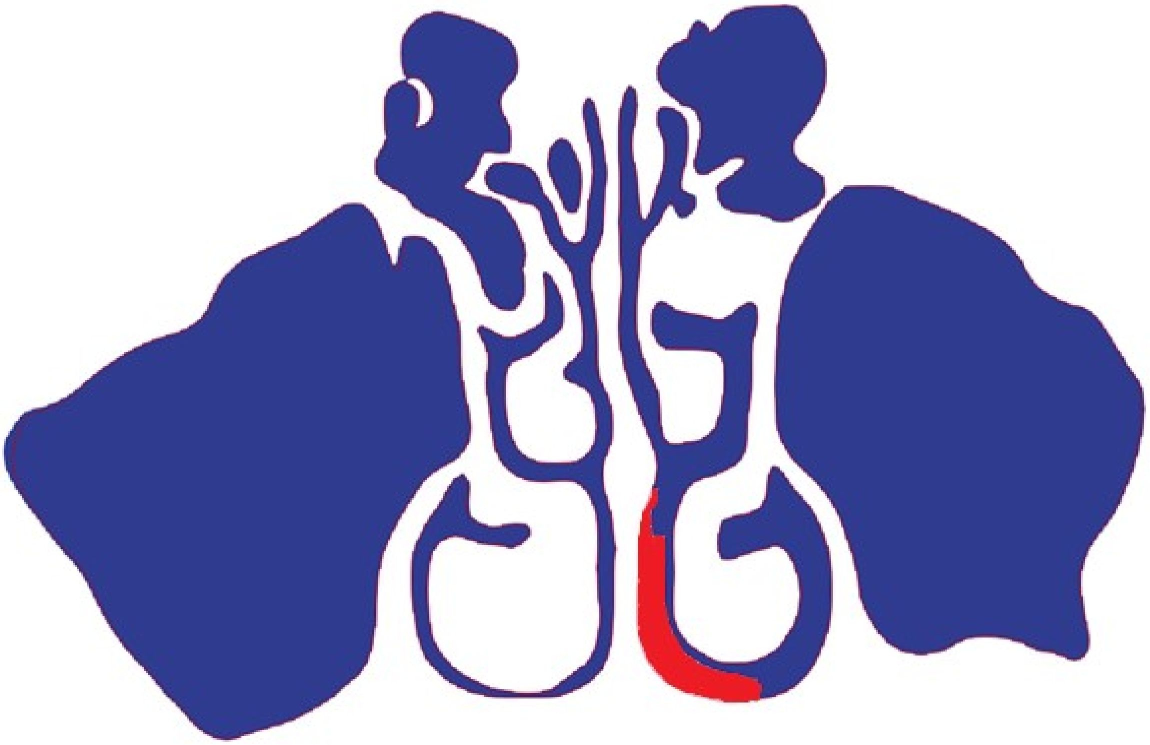

Geometry modification:

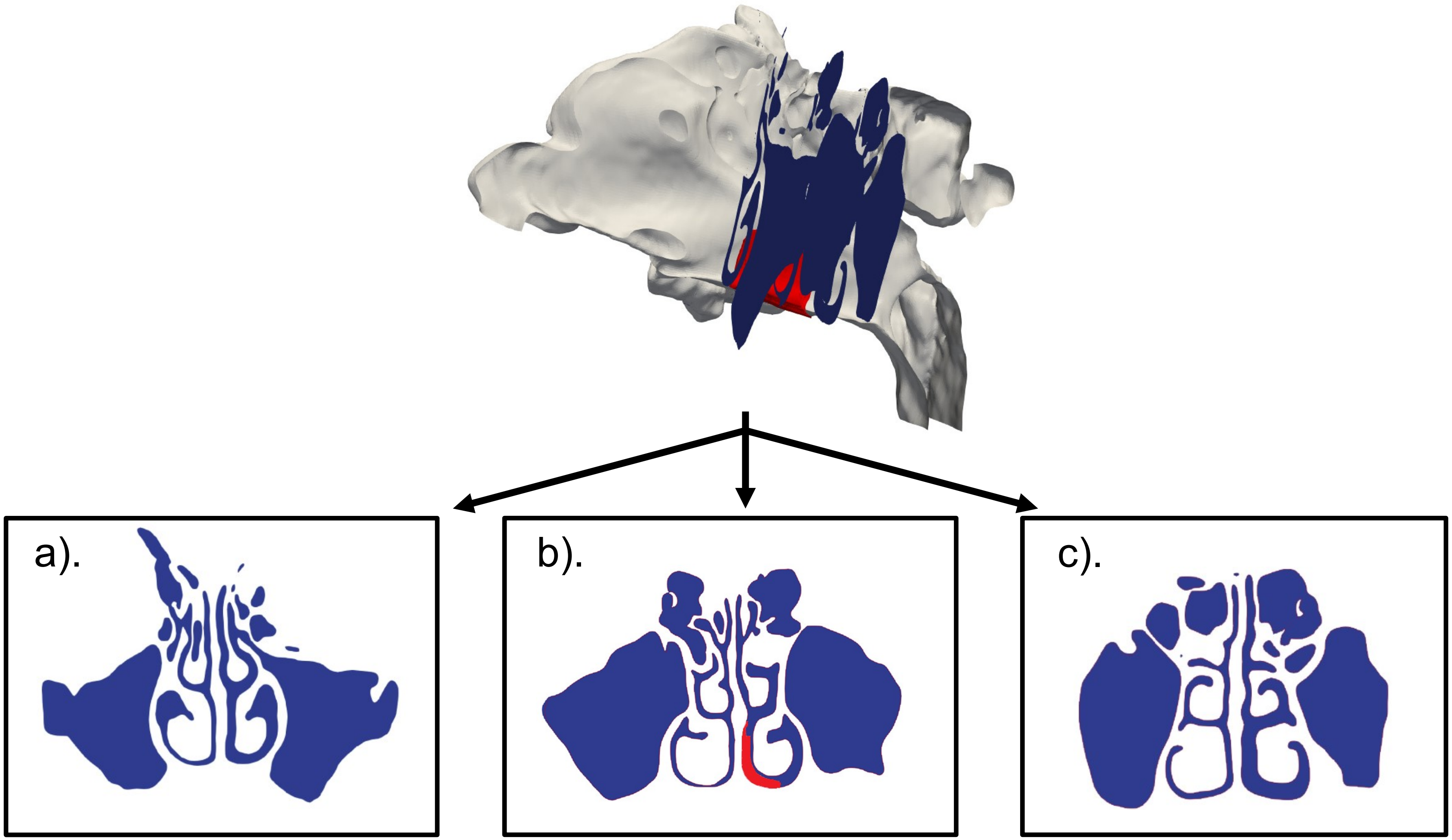

General settings:

- Three simulations are conducted in total
  - A simulations of the pre- and the postoperative geometry are performed (LBM)
  - A simulation of the virtual surgery is performed (LBM-LS)
- The highly resolved meshes contain about $100 \cdot 10^6$ cells
  - The resulting grid spacing is about $\delta x \approx 0.1mm$ (sufficient as shown in [10])
- Each simulation is advanced for 300,000 time steps
  - The results of the simulations are furthermore averaged for 300,000 time steps
- The calculations were performed on the JURECA Supercomputer in Jülich and on the CLAIX Supercomputer of RWTH Aachen
  - In total 2048 processes were employed per simulation (about 10h-15h)

Boundary Conditions:

- Nostrils:
  - Equation of St. Venant and Wantzel [1]
  - Ambient Temperature ($T_{in} = 20\ °C$)

$$\rho = \left(1 - \frac{\gamma-1}{2\gamma}\frac{3}{\rho_{t-1}^2}(\rho_{t-1}v_{t-1})^2\right)^{\frac{\gamma}{\gamma-1}}$$

- Pharynx:
  - Volume flux is prescribed by setting the corresponding Reynolds number ($\dot{V} = 250\ \frac{ml}{s}$)
  - Iterative procedure for pressure calculation [10]

- Inner walls:
  - Interpolated Bounce-Back-Scheme [6]
  - Temperature is set to body temperature [10] ($T_{Body} = 36\ °C$)

Outline

- Motivation
- Numerical Methods
- Geometry Modification & Simulation Setup
- Results
- Conclusions and Outlook

Comparison of pre- and postoperative simulation results:

- For all simulations similar setups have been used
  - The Reynolds number $Re = 808$ is based on the pharynx geometry, the volume flux in the pharynx, and the kinematic viscosity of air
- The fluid mechanical properties analyzed are:
  - The static pressure loss between nostrils and pharynx $\Delta p_s = p_{s,n} - p_{s,p}$
  - The total pressure loss between nostrils and pharynx $\Delta p_t = p_{t,n} - p_{t,p}$
  - The temperature difference between nostrils and pharynx $\Delta T = T_p - T_n$
  - The velocity and temperature distributions

Comparison of pre- and postoperative simulation results:

		Preoperative nasal cavity	Postoperative nasal cavity	Comparison
Static pressure loss	Right cavity	32.62 Pa	22.76 Pa	-43.32%
	Left cavity	28.55 Pa	27.95 Pa	-2.15%
Total pressure loss	Both cavities	30.86 Pa	25.84 Pa	-19.43%
Temperature difference	Both cavities	15.5°C	14.9°C	-4.02%
Absolute temperature	Pharynx	35.5°C	34.9°C	-

Tab 1: Comparison of the pre- and postoperative nasal cavity

Comparison of pre- and postoperative simulation results:

		Preoperative nasal cavity	Postoperative nasal cavity	Comparison
Static pressure loss	Right cavity	32.62 Pa	22.76 Pa	-43.32%
	Left cavity	28.55 Pa	27.95 Pa	-2.15%
Total pressure loss	Both cavities	30.86 Pa	25.84 Pa	-19.43%
Temperature difference	Both cavities	15.5°C	14.9°C	-4.02%
Absolute temperature	Pharynx	35.5°C	34.9°C	-

Tab 1: Comparison of the pre- and postoperative nasal cavity

Comparison of pre- and postoperative simulation results:

		Preoperative nasal cavity	Postoperative nasal cavity	Comparison
Static pressure loss	Right cavity	32.62 Pa	22.76 Pa	-43.32%
	Left cavity	28.55 Pa	27.95 Pa	-2.15%
Total pressure loss	Both cavities	30.86 Pa	25.84 Pa	-19.43%
Temperature difference	Both cavities	15.5°C	14.9°C	-4.02%
Absolute temperature	Pharynx	35.5°C	34.9°C	-

Tab 1: Comparison of the pre- and postoperative nasal cavity

Comparison of pre- and postoperative simulation results:

		Preoperative nasal cavity	Postoperative nasal cavity	Comparison
Static pressure loss	Right cavity	32.62 Pa	22.76 Pa	-43.32%
	Left cavity	28.55 Pa	27.95 Pa	-2.15%
Total pressure loss	Both cavities	30.86 Pa	25.84 Pa	-19.43%
Temperature difference	Both cavities	15.5°C	14.9°C	-4.02%
Absolute temperature	Pharynx	35.5°C	34.9°C	-

Tab 1: Comparison of the pre- and postoperative nasal cavity

Velocity distribution:

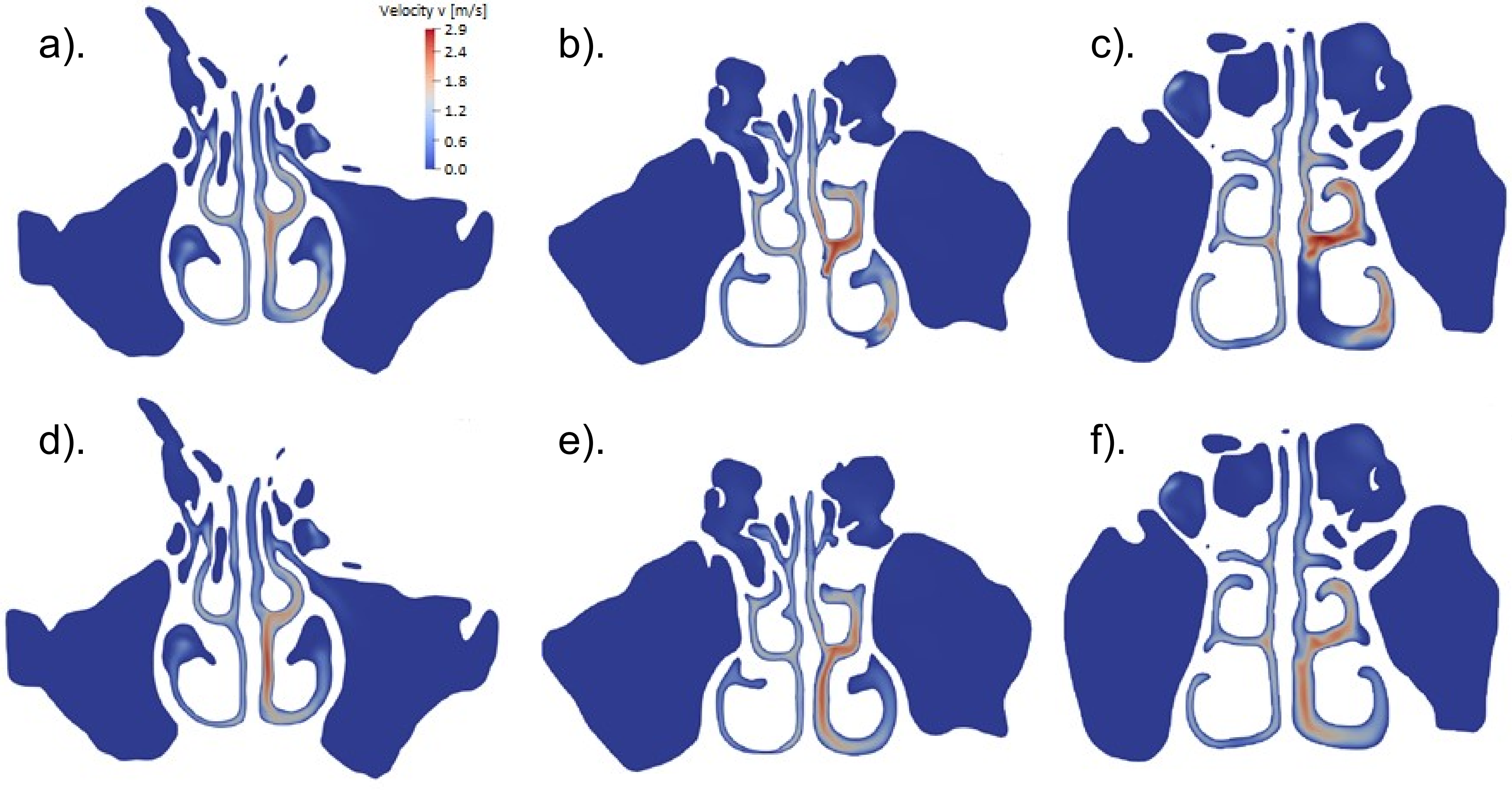

Fig 12: Velocity distribution in the slices of the pre- and postoperative simulation

Results

<u>Temperature distribution:</u>

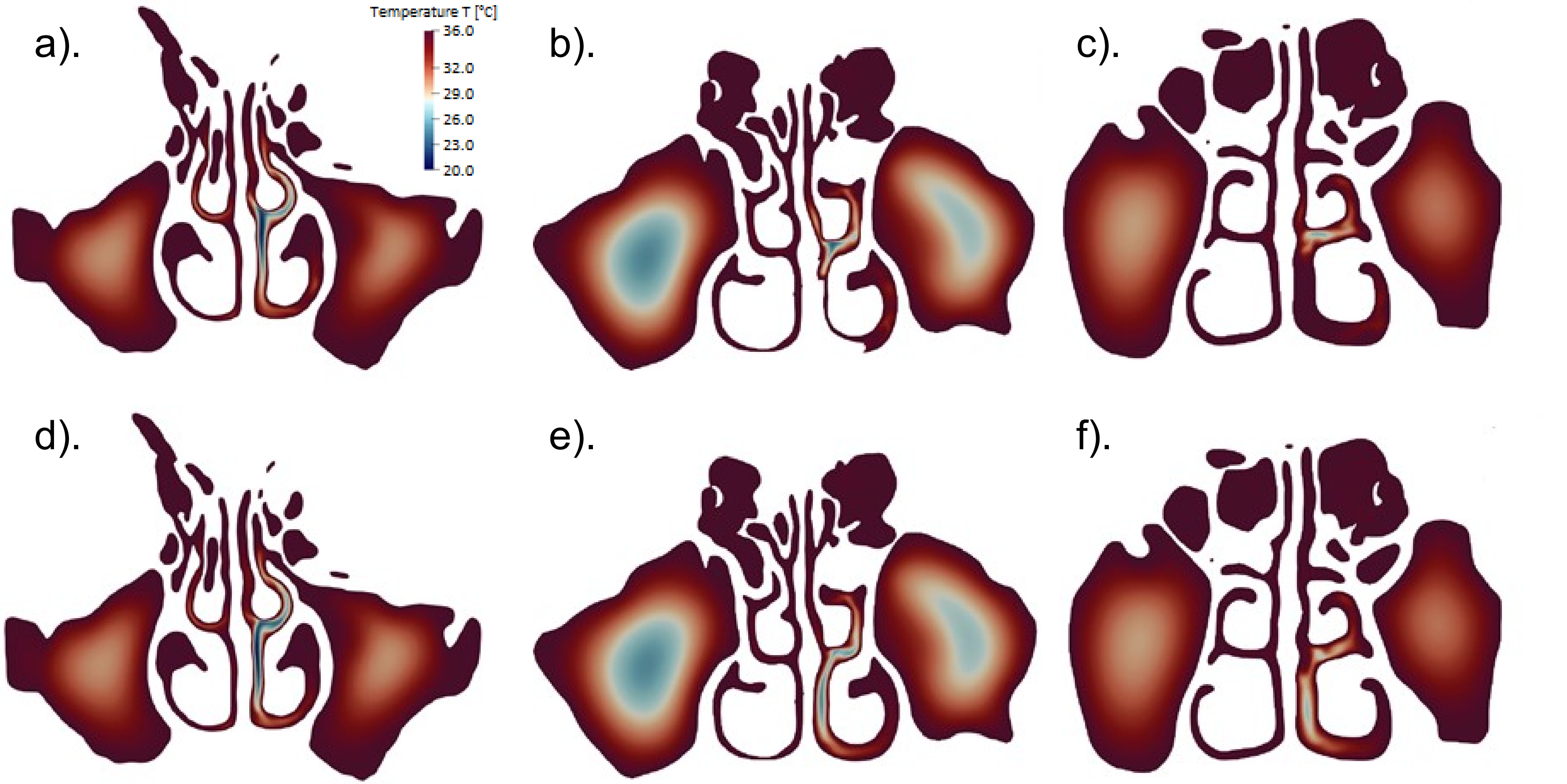

Fig 13: Temperature distribution in the slices of the pre- and postoperative simulation

Virtual surgery, temporal changes of the LS-field:

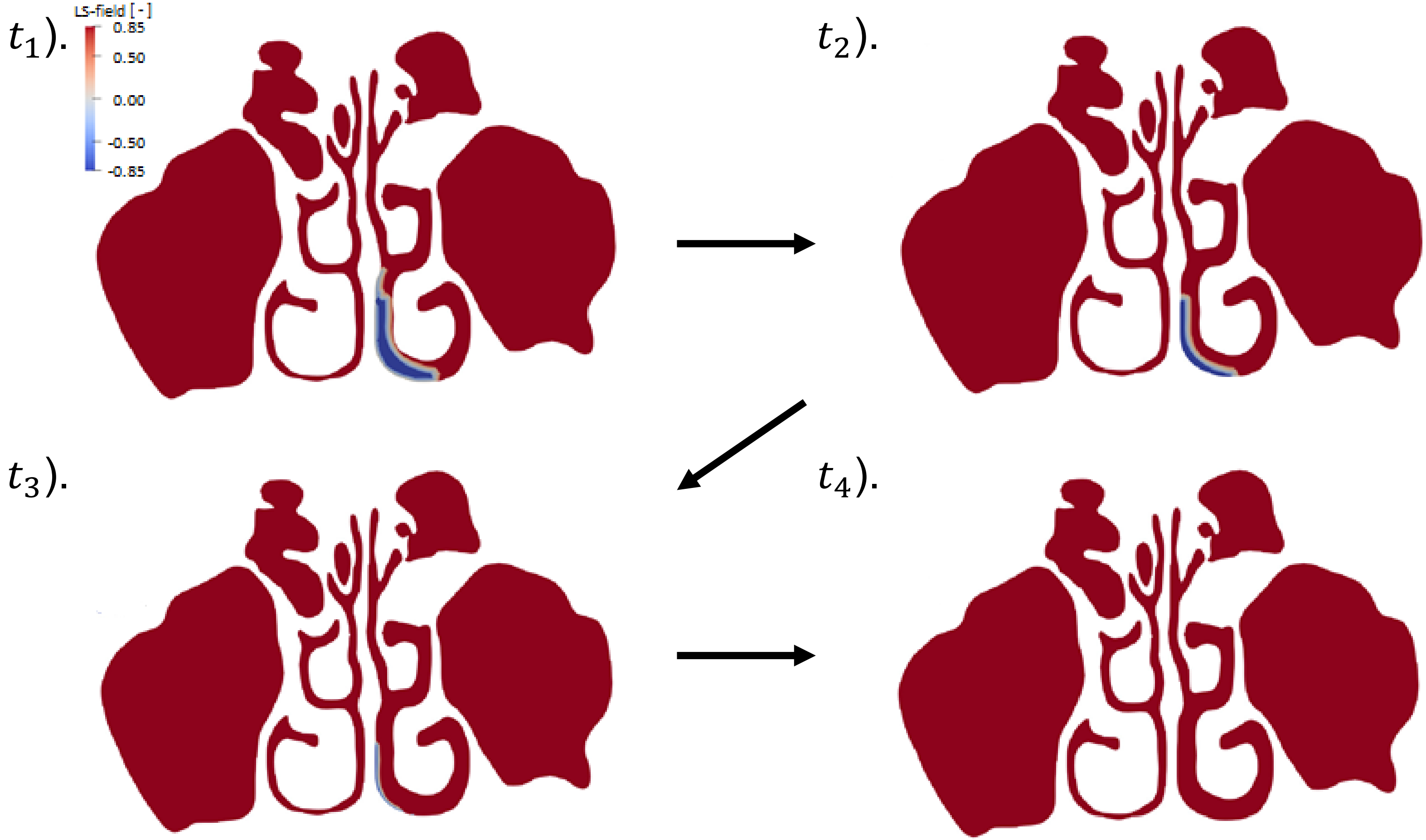

Fig 14: LS-field at four different time steps t_1 - t_4

Pressure and temperature evolution during virtual surgery:

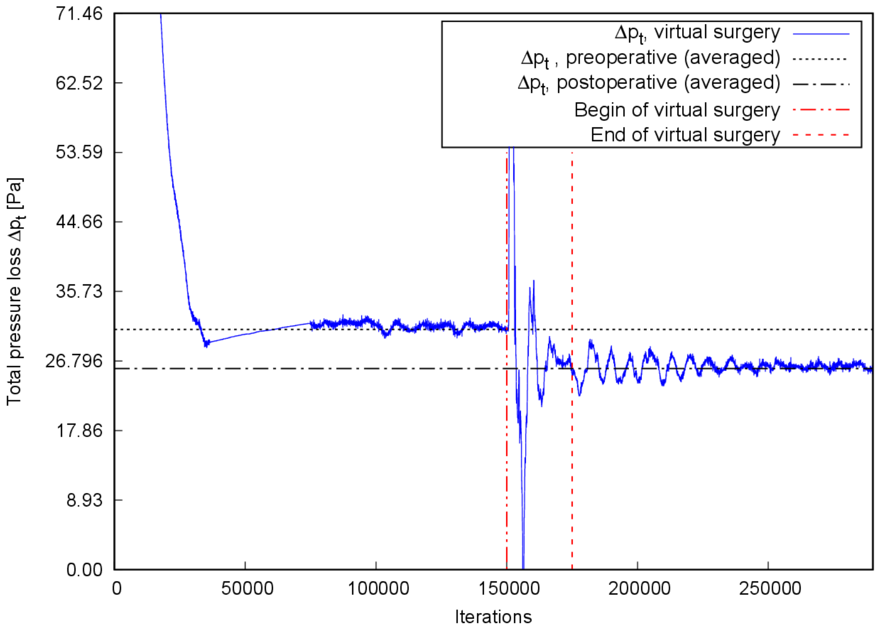

Fig 15: Comparison of the total pressure for the simulations of the pre- and postoperative nasal cavity, and the virtual surgery

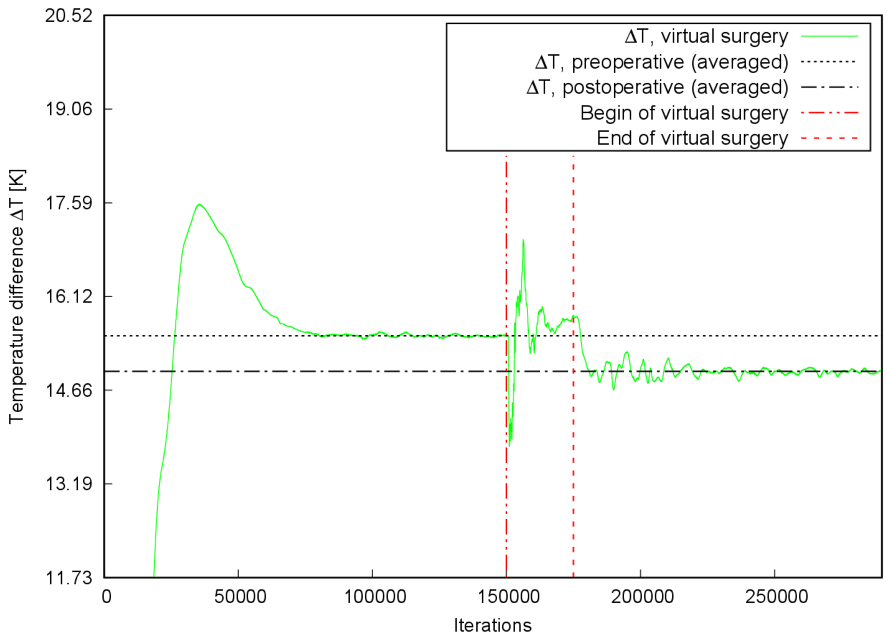

Fig 16: Comparison of the temperature for the simulations of the pre- and postoperative nasal cavity, and the virtual surgery

Outline

- Motivation
- Numerical Method
- Simulation Setup
- Results
- Conclusions and Outlook

Conclusions and Outlook

Conclusions:

- A Lattice-Boltzmann solver is employed to simulate the respiratory flow in realistic geometries of the nasal cavity
- Parts of the nasal cavity to be removed by a surgery can be represented by a *Level-Set* function
- The Coupled Lattice-Boltzmann-Level-Set Approach can be used to:
  - Conduct virtual surgeries
  - Simulate swelling/detumescence in the nasal cavity

Conclusions and Outlook

Further development:

- Optimization of the in-situ environment
  - In-situ visualization, Geometry modification
  - Performance optimization
- Implementation of a structure solver (Finite Cell Method)

Future applications:

- Fluid-structure-interaction inside the nasal cavity
- Simulation of moving surfaces
  - Nose collapse
  - Obstructive sleep apnea
- Simulation of particles inside the nasal cavity

References

[1] I. Hörschler, C. Brücker, W. Schröder, M. Meinke: *Investigation of the impact of the geometry on the nose flow*, European Journal of Mechanics – B/Fluids 25 (2006), DOI:10.1016/j.jcp.2014.10.002

[2] V. L. Srinivas: *Shape Optimization of a Car Body for Drag Reduction and to Increase Downforce* (2016)

[3] https://www.forschung-und-lehre.de/politik/cyberangriffe-auf-mehrere-supercomputer-2784

[4] A. Lintermann, W. Schröder. *Hierarchical Numerical Journey Through the Nasal Cavity: from Nose-Like Models to Real Anatomies*, Flow, Turbulence and Combustion (2017), DOI:10.1007/s10494-017-9876-0

[5] A. Lintermann, S. Schlimpert, J.H. Grimmen, C. Günther, M. Meinke, W. Schröder. *Massively parallel grid generation on HPC systems,* Computer Methods in Applied Mechanics and Engineering 277 (2014), DOI:10.1016/j.cma.2014.04.009

[6] D. Hänel, *Molekulare Gasdynamik, Einführung in die kinetische Theorie der Gase und Lattice-Boltzmann-Methoden,* Springer-Verlag (2004)

References

[7] C. Günther, M. Meinke, W. Schröder. *A flexible level-set approach for tracking multiple interacting interfaces in embedded boundary methods*, Computer & Fluids 102 (2014) DOI:10.1016/j.compfluid.2014.06.023

[8] D. Hartmann, M. Meinke, W. Schröder. *A strictly conservative Castesian cut-cell method for compressible viscous flows on adaptive grids*, Computer Methods in Applied Mechanics and Engineering 200 (2011), DOI:10.1016/j.cma.2010.05.015

[9] B. Le Chair, A. Hamielec, H. Pruppacher, *A Numerical Study of the Drag on a Sphere at Low and Intermediate Reynolds Numbers,* Journal of the Atmospheric Science 27 (1970)

[10] A. Lintermann, M. Meinke, W. Schröder: *Fluid mechanics based classification of the respiratory efficiency of several nasal cavieties*, Computers in Biology and Medicine 43 (2013), DOI:10.1016/j.compbiomed.2013.09.003